Experimental Demonstration of Longitudinal Power Monitoring over a Mixed Fiber Link

Experimental Demonstration of Longitudinal Power Monitoring over a Mixed Fiber Link

Dario Pilori, *Senior Member, IEEE,* Stefano Straullu, *Senior Member, IEEE,*
Antonino Nespola, *Senior Member, IEEE,* Lorenzo Andrenacci, *Graduate Student Member, IEEE,*
Stefano Piciaccia, and Gabriella Bosco, *Fellow, IEEE*

***Abstract*—This paper presents an experimental demonstration of the Linear-Least Squares Longitudinal Power Monitoring (LLS-LPM) technique over a mixed fiber link. The link is made by five spans, including four spans of G.652 Single-Mode Fiber (SMF) and one span of G.655 Non-Zero Dispersion-Shifted Fiber (NZDSF) with negative dispersion in the C-band. The study highlights the challenges posed by the negative dispersion of G.655 fiber and its impact on the convergence of the LLS-LPM algorithm. The experimental results demonstrate that the LLS-LPM algorithm can accurately estimate the power profile, only in the link portion where there is a one-to-one relation between the cumulated chromatic dispersion and the distance. This work provides valuable insights into the application of LLS-LPM in real-world fiber networks with mixed fiber types.**

***Index Terms*—Optical fiber communications, Longitudinal Power Monitoring, Non-Zero Dispersion-Shifted Fiber.**

I. Introduction

LONGITUDINAL Power Monitoring (LPM) is a powerful Optical Performance Monitoring (OPM) technique that facilitates advanced network troubleshooting and optimization [1], without relying on external monitoring devices, such as OTDRs. Specifically, the Linear-Least Squares (LLS) LPM technique [2] allows a direct estimation of the power profile of a Wavelength Division Multiplexing (WDM) channel. This capability not only helps in detecting anomalies, such as lumped losses, but also supports a range of more advanced applications, including predictive maintenance and dynamic resource optimization [3]. However, in almost all experimental demonstrations, LPM has been tested on homogeneous fiber links, i.e. links composed of a single fiber type, mostly G.652 Single-Mode Fiber (SMF) or G.654 Pure-Silica Core Fiber (PSCF) [4]. In such scenarios, determining the optimal step size Δz for the LPM algorithm is straightforward, as it can be directly derived from the fiber's parameters [5]. Moreover, the chromatic dispersion parameter β_2 can be estimated by dividing the total cumulated dispersion by the link length, without any knowledge of the installed fiber types.

In reality, many installed fiber networks still contain spans composed of fiber types different from SMF, in particular by Non-Zero Dispersion-Shifted Fiber (NZDSF), classified as ITU-T G.655. This fiber is particularly challenging for the LLS-LPM algorithm due to its low chromatic dispersion, which significantly reduces the spatial resolution of the power profile estimation [5]. In [6], the authors used a backpropagation-based method to identify the position of DSF and NZDSF segments within an optical link. A similar result was achieved in [7] using a correlation-method (CM) LPM.

Notably, some G.655 fibers have a negative dispersion coefficient in the C-band. When such fibers are deployed alongside SMF fiber in a mixed link, they partially compensate for the chromatic dispersion. This partial compensation disrupts the assumptions underlying the LLS-LPM algorithm, often leading to failures in the power profile estimation [2]. To the best of our knowledge, no demonstration of LPM has been reported for a partially-compensated link.

In this work, we present the first experimental demonstration of LLS-LPM over a 5-span mixed fiber link, composed of four SMF spans and one G.655 fiber spans. The G.655 fiber exhibits negative dispersion in the C-band and near-zero dispersion in the L-band. We show that the LLS-LPM algorithm successfully reconstructs the power profile in the portions of the link where there is a one-to-one relation between the distance and the cumulated chromatic dispersion. When this does not happen, we refer to this condition as "ambiguous".

II. Methodology

The LLS-LPM algorithm estimates the power profile by computing the following expression [2]:

$$\hat{\boldsymbol{\gamma}}' = \left(\mathrm{Re}\left[\boldsymbol{G}^{\dagger}\boldsymbol{G}\right]\right)^{-1}\mathrm{Re}\left[\boldsymbol{G}^{\dagger}\boldsymbol{A}_1\right]. \tag{1}$$

$\boldsymbol{G}$ is a key matrix whose structure directly affects the success of the estimation. In particular, the columns of $\boldsymbol{G}$ must be linearly independent to ensure that the matrix inversion is well defined and numerically stable [2, Sec. II-F]. According to the first-order regular perturbation theory, each column of the martix $\boldsymbol{G}$ represents the effect of chromatic dispersion applied from the input ($z = 0$) to an intermediate distance z_k, followed by a non-linear operator, and then additional dispersion from z_k to the end of the link ($z = L$). This means that, for the columns to be independent, the cumulated dispersion must vary monotonically along the link – either increasing or decreasing with distance. However, in links composed of mixed fiber types, with both positive and negative dispersion coefficients, this monotonicity condition is not satisfied.

D. Pilori, L. Andrenacci and G. Bosco are with Dipartimento di Elettronica e Telecomunicazioni (DET), Politecnico di Torino, 10129 Torino, Italy. E-Mail: dario.pilori@polito.it.

S. Straullu and A. Nespola are with LINKS Foundation, 10138 Torino, Italy.

S. Piciaccia is with CISCO Photonics Italy S.r.l., 20871 Vimercate (MB), Italy.

Manuscript received 28 May 2025; revised 3 July 2025.

TABLE I
LINK FIBER PARAMETERS AT 193.3 THz

Span	Type	L [km]	D_λ [ps/(nm · km)]
1	G.652	86.9	+16.21
2	G.652	85.6	+16.52
3	G.652	85.6	+16.34
4	G.652	86.3	+16.33
5	G.655	82.1	-2.59
Link	-	426.5	-

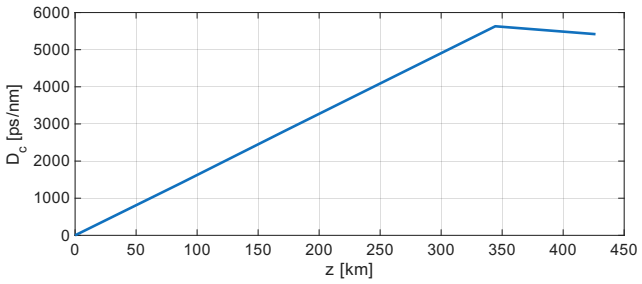

Fig. 1. Cumulated dispersion in the link at 193.3 THz (1550.9 nm).

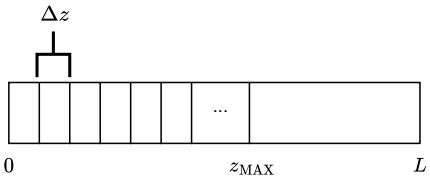

Fig. 2. Steps of the LLS-LPM algorithm [2] along the link from $z = 0$ up to $z = L$.

For example, let us consider a $L = 426.5$-km link composed of 5 spans; the first 4 are G.652 SMF, while the final span consists of a G.655 NZDSF fiber with negative dispersion in the C-band. The fiber parameters, computed at 193.3 THz (~ 1550.9 nm) are summarized in Table I, and the cumulated dispersion in the link is shown in Fig. 1. In this configuration, the dispersion increases monotonically through the four SMF spans, but then decreases in the final span due to the negative dispersion of the G.655 fiber. As a result, there is a one-to-one correspondence between propagation distance and accumulated dispersion only up to $z_A = 331.4$-km, which lies within the fourth span. Beyond this point, pairs of distinct locations in the link exhibit the same total dispersion. Consequently, the $\boldsymbol{G}$ matrix constructed over the entire link becomes ill-conditioned. However, if the matrix is computed using only the portion of the link up tp z_A, it may remain well-conditioned. This enables the LLS-LPM algorithm to accurately estimate the power profile up to that distance.

To address this issue, we propose dividing the link into N_s segments, as shown in Fig. 2. The first $N_\mathrm{s} - 1$ segments are regularly spaced with a step size Δz, while the final segment spans a larger interval, from $z_\mathrm{MAX} = (N_\mathrm{s} - 1)\Delta z$ to the total link length L. If this last, extended step includes the region where dispersion becomes ambiguous, the resulting $\boldsymbol{G}$ matrix may be better conditioned, potentially enabling convergence of the LLS-LPM algorithm. This operation, obviously, requires the knowledge, at the receiver, of the dispersion map of the link. This can be either known *a priori*, or estimated [7].

III. EXPERIMENTAL SETUP AND RESULTS

A. Setup

To validate the approach described in the previous section, we set up an experiment, whose schematic is shown in Fig. 3. The transmitter generates a 18-channel WDM comb in the C-band, with 175 GHz spacing and running at ~ 118 GBaud per channel. The channel under test (CUT), which is at the center of the WDM comb at 193.3 THz, is generated by a commercial transceiver (Acacia CIM 8) and modulated with Quadrature Phase-Shift Keying (QPSK). The other channels are emulated using shaped Amplitude Spontaneous Emission (ASE) noise [8]. The transmitted power is set to $+3$ dBm per channel, which is close to the optimum value that minimizes the Bit Error Ratio (BER). The comb is transmitted through a fiber link composed of five spans, whose parameters are summarized in Table I. Each span is followed by an Erbium-Doped Fiber Amplifier (EDFA) that fully recovers the span loss. At the receiver, an optical band-pass filter selects the CUT, which is then received by a CIM 8 coherent receiver and processed with the card's real-time DSP. From the DSP output, we periodically extract 100 blocks, each 12 288 samples long, of the received constellation after equalization and phase recovery. These constellations, along with the cumulated dispersion values, serve as input to the LLS-LPM algorithm, which is run with a spatial resolution $\Delta z = 1$ km. The LLS-LPM algorithm was run at two samples per symbol, using a root-raised-cosine shaping filter with a 10% roll-off, which is the same filter used in the commercial transceiver. The reference signal is generated by applying hard decision to the received constellation. Given the high OSNR and the use of the QPSK modulation format, the received constellation is almost error-free (BER $\sim 10^{-8}$); consequently, the decision errors had a negligible effect on the estimated power profile [9].

B. Results and Discussion

We begin our analysis by evaluating the condition number of the $\boldsymbol{G}$ matrix, defined as the ratio between the largest and the smallest singular value, for different values of z_MAX. This parameter represents the maximum distance before the last step of the LLS algorithm, as illustrated in Fig. 2. The resulting condition number is shown in Fig. 4 (right axis, red curve), along with a magnified view of of the dispersion map for reference. For small values of z_MAX, the matrix condition number remains small, since the final step of the algorithm fully includes the G.655 span. As z_MAX approaches $z_A = 331.4$ km, the condition number slightly increases, but the matrix $\boldsymbol{G}$ can be still inverted. Once z_MAX exceeds the beginning of the G.655 span (344.4 km), the condition number rapidly increases, indicating a significant deterioration in matrix conditioning. To better illustrate this effect, Fig. 5 shows three of the rows of the matrix $\boldsymbol{G}^\dagger\boldsymbol{G}$, which correspond to the spatial impulse response of the LLS-LPM algorithm [5]. The algorithm was run over the entire link ($z_\mathrm{MAX} = L$), with a spatial resolution $\Delta z = 1$ km. When estimating the optical

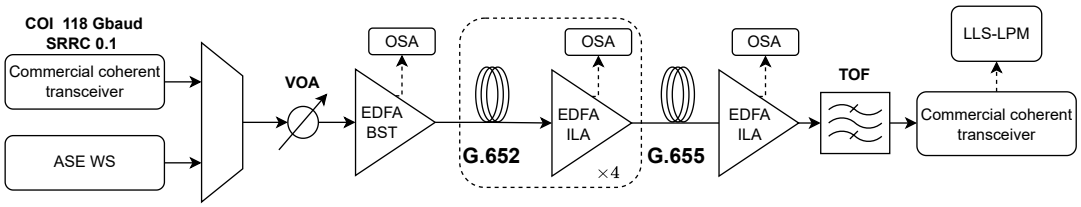

Fig. 3. Experimental setup. COI: Channel Of Interest. SRRC: Square-Root Raised Cosine. ASE WS: Amplified Sponaneous Emission WaveShaper. VOA: Variable Optical Attenuator. OSA: Optical Spectrum Analyzer. BST: Booster Amplifier. ILA: In-Line Amplifier. TOF: Tunable Optical band-pass Filter.

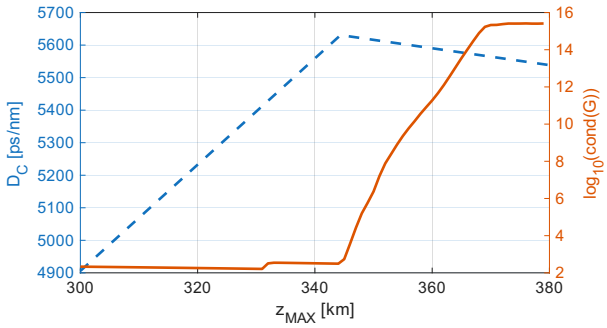

Fig. 4. Condition number of the $\boldsymbol{G}$ matrix (right axis, red solid line), along with a magnification of the cumulated dispersion of Fig. 1 (left axis, blue dashed line).

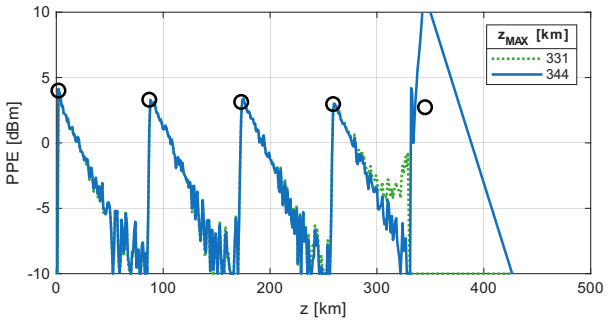

Fig. 6. Link power profile estimated by LLS-LPM with two different values of z_{MAX}. Black circles: power measurements with a power meter.

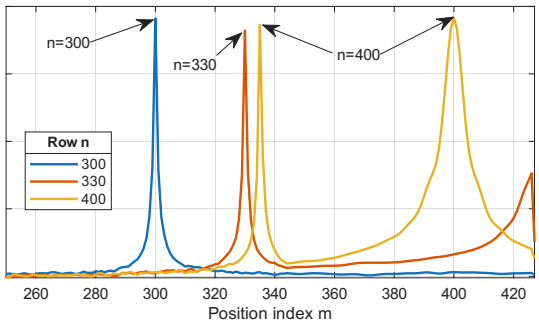

Fig. 5. Three examples of the spatial impulse response of the LLS-LPM algorithm, run over the entire link with a constant $\Delta z = 1$ km.

power in a point of the link before z_A (e.g., at $z = 300$ km), the spatial impulse response has a single peak centered at the correct distance ($m = 300$). Instead, when approaching the ambiguity point (e.g. at $z = 330$ km), a spurious peak at the end of the link appears. In the G.655 span, for instance at $z = 400$ km, the spatial impulse response has two distinct peaks. One peak, larger due to the smaller β_2, at $m = 400$, and another spurious peak appears at a shorter distance. This is the reason why the condition number of the $\boldsymbol{G}$ is high, which makes the matrix inversion in (1) numerically unstable.

The power profile estimated by the LLS-LPM algorithm, averaged over 100 different constellation blocks [10], is shown in Fig. 6, for two different values of z_{MAX}. The first value, $z_{\mathrm{MAX}} = 331$ km (blue line), corresponds to the minimum condition number identified in Fig. 4, while the second, $z_{\mathrm{MAX}} = 344$ km (red line), lies just before the start of the G.655 span. The black circles are the reference power values, measured at the output of each EDFA. The results show that the LLS-LPM algorithm correctly estimates the power profile across the first three spans, except near the beginning of the link, where the modulation-format dependence of the algorithm [5] slightly reduces its accuracy. Beyond the ambiguity point $z_A = 331$ km, the estimates degrade for both values of z_{MAX}, consistent with the theoretical requirement that the algorithm performs reliably only when there is a one-to-one correspondence between propagation distance and cumulated dispersion. The two curves differ only in the second portion of the fourth span, where the blue curve ($z_{\mathrm{MAX}} = 331$ km) becomes inaccurate. We attribute this to the spatial impulse response associated with the last – large – step, which depends on the step size [11]. A comprehensive theoretical analysis, e.g. using the framework presented in [5], is needed to properly model this effect and investigate the fundamental limitations of LLS-LPM under these conditions.

C. Moving the G.655 span

To further validate our approach, we slightly changed the experimental setup of Fig. 3, by repositioning the G.655 span *at the beginning* of the link. We then applied the LLS-LPM algorithm using the same methodology described above. In this case, rather than placing the large step at the end of the link, we introduced it at the beginning, followed by uniform steps of $\Delta z = 1$ km. Similar to before, the initial step size was set to approximately match the length of the G.655 span (83 km). The result is reported in Fig. 7, which shows the estimated power profile (red line, right axis) and the corresponding dispersion map (blue line, left axis). Notably, a one-to-one relationship between the cumulated dispersion and the propagation distance is present from ~ 95 km to the end of the link. As expected, the power profile estimation becomes

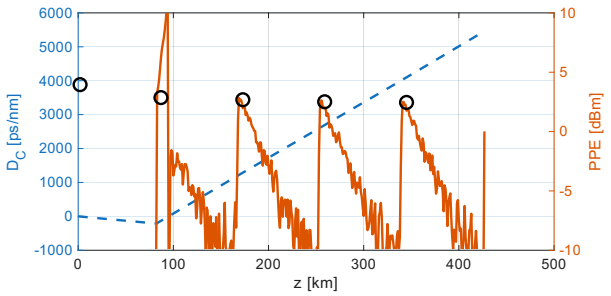

Fig. 7. Link power profile estimated by LLS-LPM (right axis, red solid line), where the G.655 span was put at the beginning of the link. The dispersion map (left axis, blue dashed line) is added as a reference. Black circles: power measurements with a power meter.

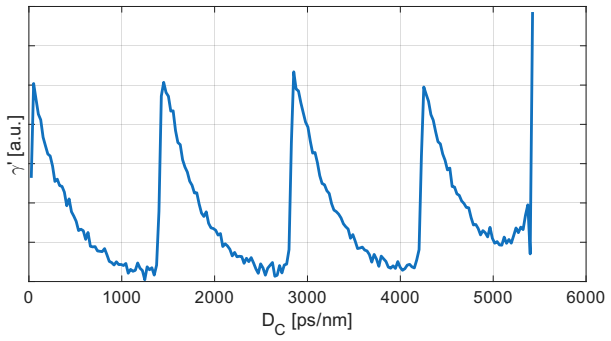

Fig. 8. Normalized power profile (γ'), with a z axis uniformly sampled in terms of cumulated dispersion.

accurate starting from this point, as it can be clearly seen from Fig. 7.

D. Estimating the position of the G.655 span

In this work, we always assumed that the link characteristics – namely, fiber type, dispersion and span length – are known at the receiver. However, if this information is unavailable, the LLS-LPM algorithm can still be applied by constructing a z axis that is uniformly spaced in terms of chromatic dispersion. This approach only requires knowledge of the total accumulated dispersion at the receiver, which is typically estimated to perform Electronic Dispersion Compensation (EDC). An example of this approach is shown in Fig. 8. Instead of showing the power profile, we show the γ', since we assume that the γ parameter of the spans is also unknown. The spatial resolution was approximately 25 ps/nm. The results show that, for the first three spans, the estimation is qualitatively accurate. Beyond that point, the accuracy degrades, and the final span is entirely undetected, since it falls entirely within the ambiguous region. Nevertheless, a sudden increase in the value of γ' suggests an increase of the optimal power, or an increase of the fiber's γ. Assuming that the amplifiers operate within the normal range, this strongly indicates that the last span is composed by a different fiber type with a significantly higher γ than SMF. This outcome is consistent with the findings in [7], although that study employed a CM-LPM method. Unfortunately, without further details about the dispersion map and link configuration, no additional insights can be extracted from this result.

IV. Conclusion

In this work, we have experimentally demonstrated the application of the LLS-LPM algorithm in a mixed-fiber link, comprising fibers with both positive and negative dispersion in the C-band. Our results show that the LLS-LPM algorithm provides accurate estimations in link segments where a one-to-one correspondence exists between the cumulated chromatic dispersion and the propagation distance. On fully dispersion-managed links, the algorithm would fail, as predicted in [2]. To mitigate the ill-conditioning of the $\boldsymbol{G}$ matrix, we propose by-passing ambiguous dispersion regions by introducing a single, large, step in the LLS-LPM algorithm. Future work should focus on developing a theoretical framework to rigorously characterize the algorithm's performance and limitations under these conditions. Moreover, future work can apply those results to the CM method, which is also based on a part of Eq. (1).

Acknowledgment

This work was sponsored by Cisco under the SRA contract "BOOST 2025". The authors would like to acknowledge Dr. Fabrizio Forghieri from Cisco for useful discussions.

References

[1] M. R. Sena, R. Emmerich, B. Shariati, R.-P. Braun, M. Geitz, J. K. Fischer, and R. Freund, "Link tomography: A tool for monitoring optical network and designing digital twins," in *ECOC 2024; 50th European Conference on Optical Communication*, 2024, pp. 176–179.

[2] T. Sasai, M. Takahashi, M. Nakamura, E. Yamazaki, and Y. Kisaka, "Linear least squares estimation of fiber-longitudinal optical power profile," *Journal of Lightwave Technology*, vol. 42, no. 6, pp. 1955–1965, 2024.

[3] A. May, F. Boitier, and P. Layec, "Advanced optical link tomography for optical network monitoring," in *Optical Fiber Communication Conference (OFC) 2025*. Optica Publishing Group, 2025, p. M2C.5.

[4] M. Takahashi, T. Sasai, M. Nakamura, and E. Yamazaki, "Experimental investigation of longitudinal power profile estimation accuracy in fibre links with large effective core area," in *ECOC 2024; 50th European Conference on Optical Communication*, 2024, pp. 990–993.

[5] T. Sasai, S. Y. Set, and S. Yamashita, "Design of fiber-longitudinal optical power monitor," *Journal of Lightwave Technology*, vol. 43, no. 5, pp. 2192–2202, 2025.

[6] T. Sasai, M. Nakamura, S. Okamoto, F. Hamaoka, S. Yamamoto, E. Yamazaki, A. M. H. Nishizawa, and Y. Kisaka, "Simultaneous detection of anomaly points and fiber types in multi-span transmission links only by receiver-side digital signal processing," in *Optical Fiber Communication Conference (OFC) 2020*. Optica Publishing Group, 2020, p. Th1F.1.

[7] M. Eto, K. Tajima, K. Sone, S. Yoshida, R. Shinzaki, S. Oda, and T. Hoshida, "Fibre type identification based on power profile estimation," in *49th European Conference on Optical Communications (ECOC 2023)*, vol. 2023, 2023, pp. 127–130.

[8] T. Richter, J. Pan, and S. Tibuleac, "Comparison of WDM bandwidth loading using individual transponders, shaped, and flat ASE noise," in *Optical Fiber Communication Conference*. Optica Publishing Group, 2018, p. W1B.2.

[9] L. Andrenacci, A. Nespola, S. Straullu, Y. Jiang, S. Piciaccia, G. Bosco, and D. Pilori, "Implementation penalties for nonlinear interference estimation with linear least squares longitudinal power monitoring," in *Optical Fiber Communication Conference (OFC) 2025*. Optica Publishing Group, 2025, p. W3E.5.

[10] T. Sasai, M. Takahashi, M. Nakamura, E. Yamazaki, and Y. Kisaka, "On the signal pattern effect on fibre-longitudinal power monitor," in *ECOC 2024; 50th European Conference on Optical Communication*, 2024, pp. 160–163.

[11] T. Sasai, E. Yamazaki, and Y. Kisaka, "Performance limit of fiber-longitudinal power profile estimation methods," *Journal of Lightwave Technology*, vol. 41, no. 11, pp. 3278–3289, 2023.